



HAL
open science

Joint estimation of object and probes in vectorial ptychography

Arthur Baroni, Marc Allain, Peng Li, Virginie Chamard, Patrick Ferrand

► **To cite this version:**

Arthur Baroni, Marc Allain, Peng Li, Virginie Chamard, Patrick Ferrand. Joint estimation of object and probes in vectorial ptychography. *Optics Express*, 2019, 27 (6), pp.8143. 10.1364/OE.27.008143 . hal-02059897

HAL Id: hal-02059897

<https://amu.hal.science/hal-02059897>

Submitted on 7 Mar 2019

HAL is a multi-disciplinary open access archive for the deposit and dissemination of scientific research documents, whether they are published or not. The documents may come from teaching and research institutions in France or abroad, or from public or private research centers.

L'archive ouverte pluridisciplinaire **HAL**, est destinée au dépôt et à la diffusion de documents scientifiques de niveau recherche, publiés ou non, émanant des établissements d'enseignement et de recherche français ou étrangers, des laboratoires publics ou privés.



Distributed under a Creative Commons Attribution 4.0 International License



Joint estimation of object and probes in vectorial ptychography

ARTHUR BARONI, MARC ALLAIN, PENG LI, VIRGINIE CHAMARD,
AND PATRICK FERRAND*

Aix-Marseille Univ, CNRS, Centrale Marseille, Institut Fresnel, F-13013 Marseille, France

*patrick.ferrand@fresnel.fr

Abstract: Vectorial ptychography has been recently introduced to reconstruct the Jones matrix of an anisotropic object by means of series of ptychographic measurements performed using a set of polarized illumination probes in conjugation with various analyzers. So far, the probes were assumed to be completely known (amplitude, wavefront, state of polarization), which is rarely the case in practice. Here we address the issue of the joint estimating of the set of polarized illumination probes together with the Jones matrix of an anisotropic object in vectorial ptychography. We propose an algorithm based on a conjugate gradient strategy. Experimental results are reported, showing an improvement on the object estimate, in addition to a precise reconstruction of the probes.

© 2019 Optical Society of America under the terms of the [OSA Open Access Publishing Agreement](#)

1. Introduction

Ptychography is an imaging technique aiming at reconstructing the transmission properties of an object, namely its transmittance and induced phase shift, by means of an iterative algorithm. It exploits series of intensity diffraction patterns acquired by scanning the specimen with a finite-size coherent probe at controlled locations, and preserving a sufficient overlap between successive illuminated areas [1]. The modeling of the ptychography problem relies on a multiplicative model for the probe-object interaction, and the data redundancy allows in principle to separate the respective contributions of the probe and object to the measured signal. Algorithms like the ptychographical iterative engine (PIE) allow successful object reconstructions if the probe is perfectly known. In practice, uncertainties on the probe produce reconstruction artefacts [2], so that methods have been developed, based on a joint reconstruction of the probe together with the object. This allowed a dramatic improvement of the obtained reconstructions [3,4]. Thanks to this progress, ptychography opened new perspectives in optical microscopy for quantitative phase imaging [5–7].

Recently, we have extended the range of applications of ptychography to anisotropic materials [8]. We have revisited the ptychography strategy using a *vectorial* formalism, in order to account for the vectorial nature of the electric field probing the object. Vectorial ptychography measurement involved several combinations of probes and analysis polarization states. Recorded data were processed using a reconstruction algorithm named vectorial PIE (vPIE). The vPIE was shown to be able to reconstruct the full anisotropic properties of the object, including transmittance, phase shift, retardance, and fast axis orientation, provided that the properties (amplitude, wavefront and state of polarization) of each of the three different probes were known [9].

In this article, we now address the issue of the joint estimation of the probes together with the object in the context of vectorial ptychography. As for the scalar case, this approach is expected to account for probe uncertainties, in order to provide better object reconstructions. The specificities of vectorial ptychography, i. e., the higher number of variables used to describe the object and the multiple probes, require the algorithm to be completely rewritten. Thus, we propose a strictly convergent algorithm based on a conjugate gradient strategy. An experimental

implementation is shown, which allows to observe the gain on the object reconstruction.

2. Theory

2.1. General principle

In vectorial ptychography, when a probe illuminates an object $\mathbf{O}(r)$, the exit field is written [8]

$$\boldsymbol{\psi}_{jk}(\mathbf{r}) = \mathbf{O}(r) \mathbf{p}_k(\mathbf{r} - \mathbf{r}_j), \quad (1)$$

or, more explicitly,

$$\begin{bmatrix} \psi_{jk,x}(\mathbf{r}) \\ \psi_{jk,y}(\mathbf{r}) \end{bmatrix} = \begin{bmatrix} \rho_{xx}(\mathbf{r}) & \rho_{yx}(\mathbf{r}) \\ \rho_{xy}(\mathbf{r}) & \rho_{yy}(\mathbf{r}) \end{bmatrix} \begin{bmatrix} p_{k,x}(\mathbf{r} - \mathbf{r}_j) \\ p_{k,y}(\mathbf{r} - \mathbf{r}_j) \end{bmatrix}, \quad (2)$$

where $\mathbf{p}_k(\mathbf{r} - \mathbf{r}_j)$ refers to the k -th incident polarized probe at the j -th scanning position. For the convenience of the derivations that will follow, we rewrite Eq. (1) as

$$\boldsymbol{\psi}_{jk}(\mathbf{r}) = \mathbf{P}_k(\mathbf{r} - \mathbf{r}_j) \boldsymbol{\rho}(\mathbf{r}), \quad (3)$$

with

$$\mathbf{P}_k(\mathbf{r}) = \begin{bmatrix} p_{k,x}(\mathbf{r}) & 0 & p_{k,y}(\mathbf{r}) & 0 \\ 0 & p_{k,y}(\mathbf{r}) & 0 & p_{k,x}(\mathbf{r}) \end{bmatrix} \quad (4)$$

and

$$\boldsymbol{\rho}(\mathbf{r}) = \begin{bmatrix} \rho_{xx}(\mathbf{r}) \\ \rho_{yy}(\mathbf{r}) \\ \rho_{yx}(\mathbf{r}) \\ \rho_{xy}(\mathbf{r}) \end{bmatrix}. \quad (5)$$

Equation (2) underlines two major features that distinguish vectorial ptychography from its scalar counterpart : (i) the Jones formalism, which requires that the object and the probes to be described by a four-component matrix [10] and the two-component vector, respectively, (ii) the requirement of several probes, corresponding to several states of polarization [8]. Therefore, in the following, what we will refer to as the solution \mathbf{S} of the problem is the set

$$\mathbf{S} = \{\mathbf{O}(\mathbf{r}); \mathbf{p}_k(\mathbf{r}), \forall k\} \quad (6)$$

that minimizes the following criterion

$$\mathcal{L}(\mathbf{S}) = \sum_{j,k,l} \left(\sqrt{I_{jkl}^{(\text{calc})}(\mathbf{S})} - \sqrt{I_{jkl}^{(\text{meas})}} \right)^2, \quad (7)$$

where l stands for the polarization analysis index.

In this equation, $I_{jkl}^{(\text{calc})}$ and $I_{jkl}^{(\text{meas})}$ are the calculated and measured intensity patterns, respectively, with, in average,

$$I_{jkl}^{(\text{calc})}(\mathbf{q}) = |\xi_{jkl}(\mathbf{q})|^2 + \epsilon_{kl}(\mathbf{q}), \quad (8)$$

where ϵ_{kl} is the expected contribution of the background component to the intensity patterns, and ξ_{jkl} is the far field scalar amplitude given by

$$\xi_{jkl} = \mathbf{h}_l^T \mathbf{F} \boldsymbol{\psi}_{jk}, \quad (9)$$

where T is the transpose operator, \mathbf{F} the far field propagator, and \mathbf{h}_l is the l -th polarization analysis operator of the exit field [8].

2.2. Vectorial conjugate gradient approach

Our method is based on the conjugate gradient, a strategy that is proven to be globally convergent [11], unlike ordered subset based approaches [12] such as the vPIE. Our vectorial approach is directly inferred from the formalism derived in the scalar case, however expressing the solution \mathbf{S} as a concatenated vector \mathbf{s} of all the object and probes components.

$$\mathbf{s} = \begin{bmatrix} \boldsymbol{\rho} \\ \mathbf{p} \end{bmatrix} \quad (10)$$

In this context, the solution \mathbf{s} , as updated at the n -th iteration, is written

$$\mathbf{s}^{(n+1)} = \mathbf{s}^{(n)} - \alpha^{(n)} \frac{\mathbf{d}^{(n)}}{\mathbf{D}^{(n)}}, \quad (11)$$

where the fraction stands for the element-wise division, $\alpha^{(n)}$ is the step size of the update at the n -th iteration [13], $\mathbf{D}^{(n)}$ the scaling vector that increases the convergence speed (see section 2.4) and $\mathbf{d}^{(n)}$ the correction term

$$\mathbf{d}^{(n)} = -\boldsymbol{\vartheta}^{(n)} + \beta^{(n)} \mathbf{d}^{(n-1)}, \quad (12)$$

where $\beta^{(n)}$ is the Fletcher-Reeve coefficient [11] and $\boldsymbol{\vartheta}^{(n)}$ is the gradient at the current iteration, defined by

$$\boldsymbol{\vartheta}^{(n)} = \frac{\partial \mathcal{L}(\mathbf{s}^{(n)})}{\partial \mathbf{s}}, \quad (13)$$

where $\boldsymbol{\vartheta}^{(n)}$ is the concatenated vector of all object and probes gradient components

$$\boldsymbol{\vartheta}^{(n)} = \begin{bmatrix} \frac{\partial \mathcal{L}(\mathbf{s}^{(n)})}{\partial \boldsymbol{\rho}} \\ \frac{\partial \mathcal{L}(\mathbf{s}^{(n)})}{\partial \mathbf{p}} \end{bmatrix}. \quad (14)$$

2.3. Object and probes gradients

With the definition of Eq. (7), the object gradient in Eq. (13) writes explicitly

$$\frac{\partial \mathcal{L}(\mathbf{s}^{(n)})}{\partial \boldsymbol{\rho}} = -2 \sum_{j,k} \mathbf{P}_k^{(n)\dagger} \mathbf{F}^\dagger \sum_l \mathbf{h}_l^\star \xi_{jkl} \left[\sqrt{\frac{I_{jkl}^{(\text{meas})}}{I_{jkl}^{(\text{calc})}}} - 1 \right], \quad (15)$$

where \star and \dagger denote the "complex conjugate" and "transposed complex conjugate" operators, respectively. Similarly, the gradient of the k -th probe \mathbf{p}_k is

$$\frac{\partial \mathcal{L}(\mathbf{s}^{(n)})}{\partial \mathbf{p}_k} = -2 \sum_j \mathbf{O}_j^\dagger \mathbf{F}^\dagger \sum_l \mathbf{h}_l^\star \xi_{jkl} \left[\sqrt{\frac{I_{jkl}^{(\text{meas})}}{I_{jkl}^{(\text{calc})}}} - 1 \right], \quad (16)$$

with \mathbf{O}_j the Jones matrix of the object cropped by the probe at the j -th position.

2.4. Scaling vector

The scaling vector $\mathbf{D}^{(n)}$ related to the object, denoted as $\mathbf{D}_\mathbf{O}^{(n)}$, writes

$$\mathbf{D}_\mathbf{O}^{(n)} = \begin{bmatrix} a_{xx} \sum_{j,k} p_{k,x}^{(n)} (\mathbf{r} - \mathbf{r}_j) \\ a_{xx} \sum_{j,k} p_{k,y}^{(n)} (\mathbf{r} - \mathbf{r}_j) \\ a_{yy} \sum_{j,k} p_{k,x}^{(n)} (\mathbf{r} - \mathbf{r}_j) \\ a_{yy} \sum_{j,k} p_{k,y}^{(n)} (\mathbf{r} - \mathbf{r}_j) \end{bmatrix}, \quad (17)$$

with $a_{xx} = \sum_l |h_{l,x}|^2$, $a_{yy} = \sum_l |h_{l,y}|^2$. The equivalent scaling vector $\mathbf{D}^{(n)}$ related to the probes, denoted as $\mathbf{D}_p^{(n)}$, is the same for all probes and writes

$$\mathbf{D}_p^{(n)} = \text{diag} \left[\sum_j \mathbf{O}_j^\dagger \begin{bmatrix} a_{xx} & a_{yx} \\ a_{yx}^* & a_{yy} \end{bmatrix} \mathbf{O}_j \right], \quad (18)$$

with $a_{yx} = \sum_l h_{l,x} h_{l,y}^*$ and where diag is a function that extracts the diagonal components of the matrix.

2.5. Specific under-determinations in vectorial ptychography

In this section, we discuss how trivial under-determinations in scalar ptychography could become more problematic in vectorial ptychography.

Ptychography, in its *scalar* form, is known to be insensitive to a global phase shift or amplitude attenuation of the probe and/or object. These under-determinations are so-called trivial, because all corresponding solutions of the problem, object or probe, show *de facto* identical optical behaviors.

In *vectorial* ptychography however, these under-determinations take a generalized form that deserves to be carefully considered. Indeed, the exit field of Eq. (1) can also be written as

$$\psi_{jk}(\mathbf{r}) = \mathbf{O}(\mathbf{r}) \mathbf{M} \mathbf{M}^{-1} \mathbf{p}_k(\mathbf{r} - \mathbf{r}_j), \quad (19)$$

where \mathbf{M} is a \mathbf{r} -invariant invertible Jones matrix, corresponding to a non-absorbing optical element (waveplate, rotator, or any arbitrary stacking of these), so that the set

$$\mathbf{O}'(\mathbf{r}) = \mathbf{O}(\mathbf{r}) \mathbf{M}, \quad (20)$$

$$\mathbf{p}'_k(\mathbf{r}) = \mathbf{M}^{-1} \mathbf{p}_k(\mathbf{r}) \quad (21)$$

is another solution of the problem. Here, the optical properties of the solution $\{\mathbf{O}'; \mathbf{p}'_k\}$ could be possibly drastically different from those of $\{\mathbf{O}; \mathbf{p}_k\}$.

Thus, with this respect, vectorial ptychography appears to be more under-determined than its scalar counterpart. Nevertheless, in practice, such under-determination can be softened by a prior knowledge of some optical properties of the object \mathbf{O} and/or of the probes \mathbf{p}_k , that allows to resolve the matrix \mathbf{M} from the obtained solution. In this work, as we will see later, we will take benefit of the simple knowledge of the state of polarization (SoP) of the probes toward this end.

3. Experiments

In this section, we detail a practical implementation of our method in the optical range. The measured object was a birefringent target (R2L2S1B, Thorlabs), already described and investigated in [9].

Measurements were carried out on an inverted microscope in a selected-area configuration, offering a full control of the illumination and detection polarization states, and detailed in [9]. The illumination probes were optically defined by placing a ring iris diaphragm (SM1D12C, Thorlabs) opened at a diameter of about 2 mm in the imaging plane using a 10× objective lens (ACHN-P, NA 0.25, Olympus), offering a reasonable estimate of 200 μm for the probe diameter. The camera sensor was placed at a distance of 190 mm after the diaphragm. Note that given this short distance, a Fresnel propagator was used as far field operator in the reconstructions [14].

We used the general strategy proposed in [8] consisting of probing the object by nine combinations of three successive linearly-polarized probes at angles of 0, 45, 90° in the object plane, labelled as $k = 1, 2, 3$, and three linear analyses, with the same angles, labelled as

$l = 1, 2, 3$. The SoP of the probes was classically checked using the crossed-analyzer method, which confirmed their proper orientation, with a precision better than 1° . The ellipticity was found to be negligible, below 1%, so that all probes were assumed to be linearly polarized in the following.

The object was scanned under the probes on a grid of 200 points with average steps of $29.2 \mu\text{m}$ in both x and y directions with additional random step fluctuations of $\pm 15\%$, in order to avoid periodic reconstruction ambiguities [4].

4. Reconstruction sequence

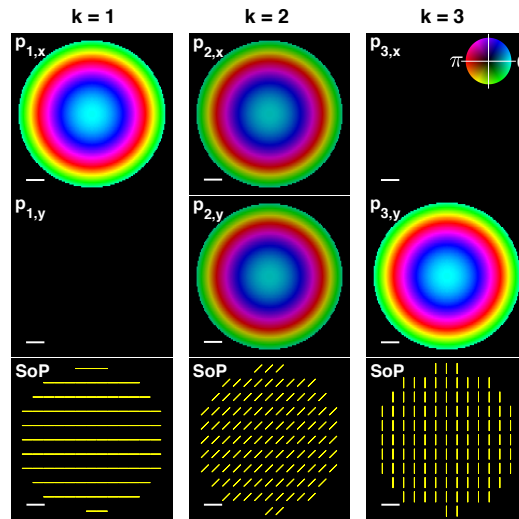


Fig. 1. Initial guess of the three probes for $k = 1$ to 3, from left to right. From top to bottom, $p_{k,x}$, $p_{k,y}$, and SoP of \mathbf{p}_k . Inset shows the complex value color coding, with phase encoded as hue and modulus as brightness. Scale bar is $25 \mu\text{m}$.

The reconstructions were performed in the following sequence:

- (i) The four components of the Jones map of the object were initialized as random amplitude ($\in [0; 1]$) and phase ($\in [0; 2\pi]$) distributions. The first estimates of the three probes were set as $200\text{-}\mu\text{m}$ diameter disks of constant amplitude, with a radial quadratic wavefront curvature estimated following the method detailed in [9], and with their known SoP. These three probes are depicted in Fig. 1.
- (ii) Reconstruction started by 30 iterations of vPIE, updating only the object. Indeed, even if the conjugate gradient method is globally convergent and more accurate than the PIE [15], this latter benefits from a fast convergence speed for the early iterations [12] and allows to produce a reasonable estimate of the object within a few iterations;
- (iii) Then, 750 iterations of conjugate gradient were applied to both object and probes, that refined the object and retrieved the probes, so that a solution $\{\mathbf{O}'; \mathbf{p}'_k\}$ is found;
- (iv) Finally, in order to release the indetermination discussed in sec. 2.5, the SoPs of the \mathbf{p}'_k was investigated and a invertible matrix \mathbf{M} was found so that the SoP of the probes $\mathbf{p}_k = \mathbf{M}\mathbf{p}'_k$ best match the known SoPs of the probes for all k 's, in agreement with Eq. (20). This allowed to retrieve the object $\mathbf{O} = \mathbf{O}'\mathbf{M}^{-1}$, in agreement with Eq. (21), and thus to return a unique set $\{\mathbf{O}; \mathbf{p}_k\}$.

The total computing time was 18 hours on a standard laptop computer.

5. Results

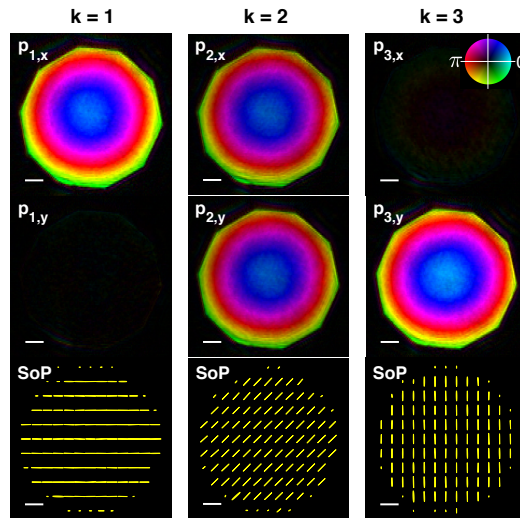


Fig. 2. Reconstructed probes \mathbf{p}_k . Same formatting as Fig. 1. Scale bar is $25 \mu\text{m}$.

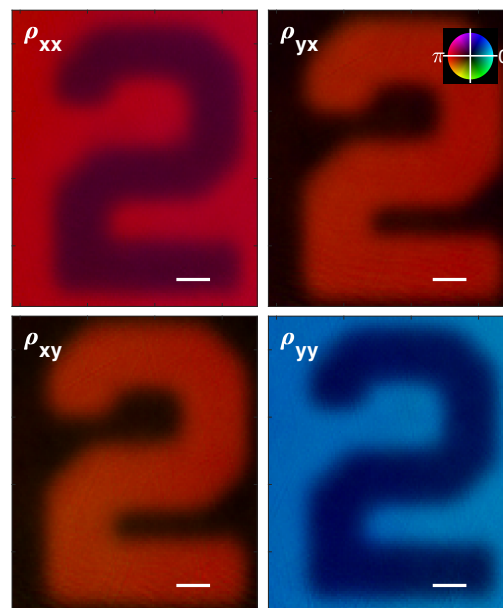


Fig. 3. Reconstructed Jones maps of the birefringent test target. Inset shows the complex value color coding, with phase encoded as hue and modulus as brightness. Scale bar is $25 \mu\text{m}$.

Following the reconstruction sequence detailed in the previous section, the set of probes \mathbf{p}_k , the SoPs of which best match the known SoPs are depicted in Fig. 2. They faithfully exhibit the

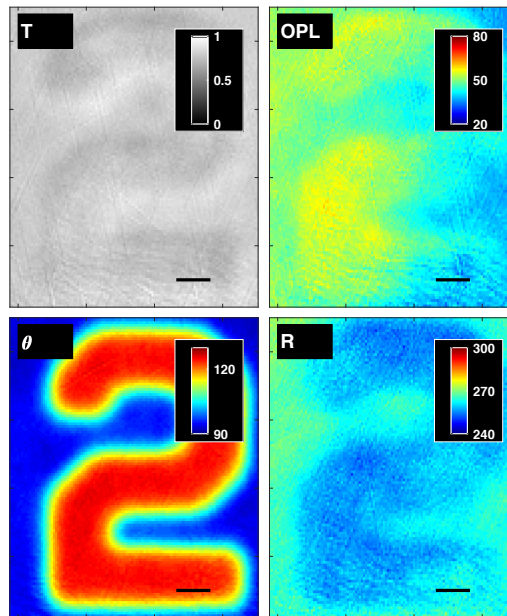


Fig. 4. Retrieved optical properties of the birefringent test target: Normalized power transmittance T , relative optical path length (OPL) variations, in nm, fast axis orientation θ , in degrees, and retardance R , in nm. Scale bar is $25 \mu\text{m}$.

correct linear-polarization orientations and a negligible ellipticity. Remarkably, the polygonal shape due to the iris diaphragm has been accurately retrieved. The wavefront curvature has decreased and a slight misalignment of the wavefront with respect to the diaphragm center was found, confirming the sensitivity of the method to account for real experimental conditions.

Close-ups of the reconstructed Jones maps of the object $\mathbf{O}(\mathbf{r})$ are depicted in Fig. 3. The main optical properties, namely the power transmittance T , the optical path length (OPL) variations, the fast axis orientation θ , and the retardance R , retrieved using the method described in [9], are depicted in Fig. 4. Reconstructed optical features exhibit uniform features, except the fast axis orientation, different inside the '2' feature and in the surrounding area, in agreement with the specific design of the object. Note that the apparent low resolution in the reconstructed object, is due to the object itself, the pattern of which is poorly defined [9].

6. Discussion

In order to demonstrate its gain in the object reconstruction, our method, now referred to as method (a), has been compared to other reconstruction strategies that do not involve any probes reconstruction, denoted methods (b) and (c). All methods share the same initial guesses and total number of iterations. As such, methods (b) and (c) mimic realistic experiments performed with a moderate level of knowledge of the shape and wavefront of the probes. They differ by the reconstruction algorithm that they use: (b) is based on a conjugate-gradient, like (a), while (c) uses the vPIE method [9]. Computing times were respectively 14 and 9 hours for methods (b) and (c).

The corresponding reconstructed objects, depicted in Fig. 5, show similar fast axis orientation and retardance maps as those of Fig. 4. However, both appear to be much less homogeneous, with a deeper depression of R in the lower central area, and show oblique hatches. Such artefacts are typical from reconstructions that are limited by an insufficient knowledge of the probes. The

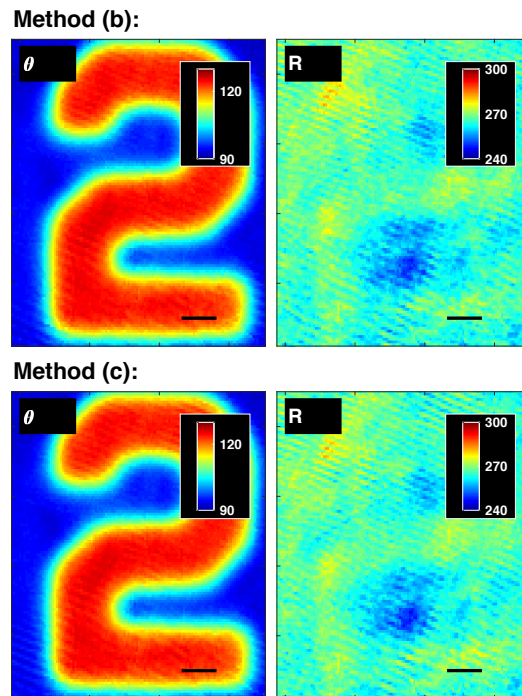


Fig. 5. Retrieved optical properties of the test target, obtained with methods (b) and (c), to be compared with Fig. 4. Scale bar is $25 \mu\text{m}$.

evolution of the criterion $\mathcal{L}(s^{(n)})$ calculated for the different methods is plotted in Fig. 6. One can observe that methods (b) and (c) have comparable convergence speed, behavior and limits, with a plateau reached after 300 iterations. Combined with the similarity of the reconstructed objects (Fig. 5(b) and 5(c)), one can conclude that, although based on different strategies, methods (b) and (c) can be considered as equivalent.

Our method (a) (Fig. 6(a)) shows a drastically different convergence behavior, namely a continuous decrease of the criterion, that one can attribute unambiguously to the joint object and probes update. Given the higher degree of freedom offered to the solution, the convergence speed is naturally lower, with a clear benefit to the reconstructed object (Fig. 4). This can be clearly attributed to the full reconstruction of the probes. Note that such level of knowledge of the probes, including the spatial distribution of their SoPs, their wavefronts, their support function, would be challenging even for a trained experimentalist.

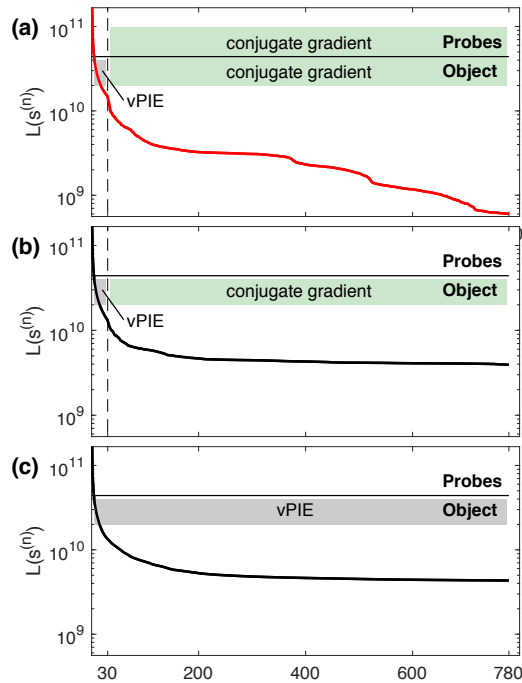


Fig. 6. Evolution of the criterion $\mathcal{L}(s^{(n)})$ for different reconstruction strategies. For each method, labelled (a) to (c), colored patterns remind which algorithm is used and which variable is updated, either the object only or both object and probes.

7. Conclusion

In this work, we have proposed an improvement of vectorial ptychography by implementing the joint estimation of the object's Jones matrix together with the vectorial probes, based on the conjugate gradient strategy. We have proposed a way to release vectorial-specific indeterminations, by simply exploiting the knowledge of the SoP of the probes. Experimental results were shown and a clear refinement on the object reconstruction, together with a faithful retrieval of the probes, were reported.

The potential of our method relies on its capacity to address specimens of any size and to its ability to image, at optical resolution, both isotropic (transmittance, OPL) and anisotropic (birefringence, diattenuation, eigenmodes) properties contained in the Jones matrix. The specificity to these two aspects opens new imaging perspectives for characterizing systems offering unusual properties, such as optical metasurfaces [16], or spatially structured for wavefront control purpose (zone plates [17], spatial light modulators [18], multicore fiber bundles [19], etc.) and involving anisotropic materials.

Funding

H2020 European Research Council (724881).

References

1. H. M. L. Faulkner and J. M. Rodenburg, "Movable aperture lensless transmission microscopy: A novel phase retrieval algorithm," *Phys. Rev. Lett.* **93**, 023903 (2004).
2. H. M. L. Faulkner and J. M. Rodenburg, "Error tolerance of an iterative phase retrieval algorithm for moveable illumination microscopy," *Ultramicroscopy* **103**, 153–164 (2005).

3. P. Thibault, M. Dierolf, A. Menzel, O. Bunk, C. David, and F. Pfeiffer, "High-resolution scanning x-ray diffraction microscopy," *Science* **321**, 379–382 (2008).
4. A. M. Maiden and J. M. Rodenburg, "An improved ptychographical phase retrieval algorithm for diffractive imaging," *Ultramicroscopy* **109**, 1256–1262 (2009).
5. J. Marrison, L. Rätty, P. Marriott, and P. O'Toole, "Ptychography – a label free, high-contrast imaging technique for live cells using quantitative phase information," *Sci. Rep.* **3**, 2369 (2013).
6. L. Shemilt, E. Verbanis, J. Schwenke, A. K. Estandarte, G. Xiong, R. Harder, N. Parmar, M. Yusuf, F. Zhang, and I. K. Robinson, "Karyotyping human chromosomes by optical and x-ray ptychography methods," *Biophys. J.* **108**, 706–713 (2015).
7. S. McDermott, P. Li, G. Williams, and A. Maiden, "Characterizing a spatial light modulator using ptychography," *Opt. Lett.* **42**, 371–374 (2017).
8. P. Ferrand, M. Allain, and V. Chamard, "Ptychography in anisotropic media," *Opt. Lett.* **40**, 5144–5147 (2015).
9. P. Ferrand, A. Baroni, M. Allain, and V. Chamard, "Quantitative imaging of anisotropic material properties with vectorial ptychography," *Opt. Lett.* **43**, 763–766 (2018).
10. R. C. Jones, "A new calculus formalism for the treatment of optical systems. I. Description and discussion of the method," *J. Opt. Soc. Am.* **31**, 488–493 (1941).
11. L. Sorber, M. Barel, and L. Lathauwer, "Unconstrained optimization of real functions in complex variables," *SIAM J. Optim.* **22**, 879–898 (2012).
12. P. Godard, M. Allain, V. Chamard, and J. Rodenburg, "Noise models for low counting rate coherent diffraction imaging," *Opt. Express* **20**, 25914–25934 (2012).
13. J. Nocedal and S. Wright, *Numerical Optimization* (Springer-Verlag, 2006), 2nd ed.
14. J. W. Goodman, *Introduction to Fourier Optics* (W. H. Freeman & Co Ltd, 2017), 4th ed.
15. M. Guizar-Sicairos and J. R. Fienup, "Phase retrieval with transverse translation diversity: a nonlinear optimization approach," *Opt. Express* **16**, 7264–7278 (2008).
16. A. V. Kildishev, A. Boltasseva, and V. M. Shalaev, "Planar photonics with metasurfaces," *Science* **339**, 1232009 (2013).
17. E. Bricchi, J. D. Mills, P. G. Kazansky, B. G. Klappauf, and J. J. Baumberg, "Birefringent Fresnel zone plates in silica fabricated by femtosecond laser machining," *Opt. Lett.* **27**, 2200–2202 (2002).
18. S. McDermott, P. Li, G. Williams, and A. Maiden, "Characterizing a spatial light modulator using ptychography," *Opt. Lett.* **42**, 371–374 (2017).
19. D. Kogan, S. Sivankutty, V. Tsvirkun, G. Bouwmans, E. R. Andresen, H. Rigneault, and D. Oron, "Phase retrieval in multicore fiber bundles," *Opt. Lett.* **42**, 647–650 (2017).